The Astrophysical Journal, 895:122 (14pp), 2020 June 1 https://doi.org/10.3847/1538-4357/ab8bd4

Looking at Blazar Light-curve Periodicities with Gaussian Processes

Stefano Covino[1], Marco Landoni[1], Angela Sandrinelli[1], and Aldo Treves[1,2]
[1] INAF/Brera Astronomical Observatory, via Bianchi 46, I-23807, Merate (LC), Italy; stefano.covino@inaf.it
[2] Università degli Studi dell'Insubria, Via Valleggio 11, I-22100 Como, Italy
Received 2019 December 13; revised 2020 April 20; accepted 2020 April 20; published 2020 June 3

Abstract

Temporal analysis of blazar flux is a powerful tool to draw inferences about the emission processes and physics of these sources. In the most general case, the available light curves are irregularly sampled and influenced by gaps, and in addition are also affected by correlated noise, making their analysis complicated. Gaussian processes may offer a viable tool to assess the statistical significance of proposed periods in light curves characterized by any sampling and noise pattern. We infer the significance of the periods proposed in the literature for two well known blazars with multiple claims of possible year-long periodicity: PG 1553 + 113 and PKS 2155–304, in the high-energy and optical bands. Adding a periodic component to the modeling gives a better statistical description of the analyzed light curves. The improvement is rather solid for PG 1553 + 113, both at high energies and in the optical, while for PKS 2155–304 at high energies the improvement is not yet strong enough to allow cogent claims, and no evidence for periodicity emerged from the analysis in the optical. Modeling a light curve by means of Gaussian processes, in spite of being relatively computationally demanding, allows us to derive a wealth of information about the data under study and suggests an original analysis framework for light curves of astrophysical interest.

Unified Astronomy Thesaurus concepts: Blazars (164); Gaussian Processes regression (1930); Lomb-Scargle periodogram (1959); Time series analysis (1916); Astrostatistics techniques (1886); Period search (1211)

1. Introduction

Blazars (e.g., Urry 2012) are some of the most frequent targets for monitoring programs at essentially any wavelength because of their variability, from the radio band to the highest energies. A natural outcome of this intense monitoring is the availability of long time series that offer a treasure of possible information about this class of sources (e.g., Ryan et al. 2019). One of the most interesting topics that can be addressed with well sampled time series is the identification of possible periodic or quasi-periodic behaviors. Several authors have indeed proposed quasi-periodic oscillations (QPO) for blazars at various levels of statistical significance (e.g., Lehto & Valtonen 1996; Sandrinelli et al. 2014, 2016a, 2016b, 2017, 2018; Zhang et al. 2014, 2017b, 2017a, 2017c; Ackermann et al. 2015; Cutini et al. 2016; Stamerra et al. 2016; Covino et al. 2017; Cavaliere et al. 2017; Prokhorov & Moraghan 2017; Tavani et al. 2018; Ait Benkhali et al. 2020; Bhatta 2019; Bhatta & Dhital 2020; Chevalier et al. 2019; Covino et al. 2019; Rieger 2019).

This interest is not misplaced, since QPOs in blazars could be powerful diagnostics of different phenomena associated to blazar phenomenologies (e.g., Lindfors et al. 2016). Interpretation of possible QPOs in blazars has recently attracted the attention of several works (e.g., Caproni et al. 2017; Cavaliere et al. 2017; Sobacchi et al. 2017; Holgado et al. 2018; Cavaliere et al. 2019; Lico et al. 2020), mainly motivated by the various claims for periodicities proposed in the last few years. One picture of interest envisages the QPOs as due to a supermassive binary black hole system. This might directly introduce periodicities in the observed emissions (e.g., Lehto & Valtonen 1996; Sandrinelli et al. 2014; Graham et al. 2015) or indirectly through precession of the whole system (Doğan et al. 2015). On the other hand, QPOs, possibly of transient nature, could also be generated by instabilities in the relativistic jets or in the accretion disks (Camenzind & Krockenberger 1992; Marscher 2014; Raiteri et al. 2017).

2. Time Series Analysis

The analysis of time series is a fundamental tool in modern astrophysics (e.g., Vaughan 2012). Given the large variety of astronomical data we can deal with, it is natural that many different techniques can be applied. Without any claim of completeness, two general scenarios can be depicted: those to treat evenly spaced data and those to cope with the irregular sampling as is the case with astronomical observations. Evenly sampled data offer the remarkable advantage to allow analyses based on a well developed set of procedures and theorems to interpret their results (e.g., van der Klis 1989, for a comprehensive review). The case of irregularly sampled data can be dealt with using the recipes developed by Lomb (1976) and Scargle (1982). The Lomb–Scargle (LS) periodogram offers a rigorous solution to the problem of detecting periodic signals in noisy time series (Bretthorst 2003; VanderPlas 2018). However, it is also known to produce distorted versions of the true periodogram and alternative approaches have also been proposed (e.g., Vio & Andreani 2018). Moreover, decomposing a light curve into harmonic series unavoidably implies a particular sensitivity to quasi-sinusoidal variations. In order to cope with periodicities with any functional form, nonparametric analysis tools have been developed (e.g., Stellingwerf 1978; Schwarzenberg-Czerny 1997; Huijse et al. 2018).

Independently of the particular analysis recipe, the problem of assessing the significance of any possible periodicity in a light curve requires one to evaluate the probability that at the frequency of interest the measured power (or any other adopted periodicity indicator) is not due, to a given confidence level, to random fluctuations. This assessment depends critically on the noise affecting the data. If we can assume the noise is "white," i.e., independent of the frequency, it is possible to compute the

exact significance level of any observed power. The most general case, red or correlated noise (Press 1978; Milotti 2002, 2007), is considerably more difficult and still an open problem. For evenly spaced data, several approaches have been suggested (e.g., Vaughan 2010; Barret & Vaughan 2012; Guidorzi et al. 2016; Vaughan et al. 2016), while for the more common unequally spaced observations only indirect procedures can be applied. There are several problems to deal with anyway. Again, with no claim of completeness for this widely debated topic, we can mention the unknown distribution of periodogram peaks, the poor measurement of population variance (Koen 1990), and the independence of the powers for a periodogram at the various frequencies. This is guaranteed only when data are evenly spaced and the periodogram is computed at the Fourier frequencies, or on any other ortho-normal frequency grid. Under this condition, a formal fit of the noise functional form is possible and inferences can be derived once the noise has been properly modeled. Otherwise, a procedure often followed consists of generating a large number of dense, long, and highly sampled simulated light curves given a set of possible noise models (or noise model parameters; Uttley et al. 2002). Then, light curves with the same sampling of the observed curve are obtained and statistics about the power of the derived periodograms are obtained (e.g., Ackermann et al. 2015; Graham et al. 2015; Bhatta 2019; Nilsson et al. 2018; Tavani et al. 2018). Other approaches are of course possible, depending on the specific data set in the analysis. As a matter of fact, the fundamental problems of assessing the significance of peaks in astronomical periodograms have understandably always received great attention in literature (e.g., Baluev 2008; Süveges et al. 2015; Hara et al. 2017; Sulis et al. 2017).

An alternative procedure is to derive information about possible periodic behaviors working in the time rather than frequency domain (e.g., Li & Wang 2018; Feigelson et al. 2018). While often computationally expensive, working in the time domain presents several advantages. First of all, one can apply inferences with data with uncertainties normally distributed. This is not (in general) the case in the frequency domain (Israel & Stella 1996). In addition phenomena affecting analysis in the frequency domain, such as leakage, aliasing, etc., are unimportant or much easier to deal with. The inferences are also often made less ambiguous since one does not have to rely on asymptotic behaviors, statistical tests strictly holding only for infinite time series, or hypotheses of stationarity (Kwiatkowski et al. 1992).

An effective approach to time series modeling in the time domain has been developed to check if the observed data can be generated by autoregressive processes (Koen 2005; Kelly et al. 2009, 2014; Feigelson et al. 2018; Lenoir & Crucifix 2018; Takata et al. 2018; Elorrieta et al. 2019; Kovačević et al. 2019). It is indeed well known that if the noise is correlated then spurious and transients quasi-periodicities can be observed (e.g., Vaughan et al. 2016). A partly different procedure that is becoming increasing popular in the astronomical literature (e.g., Brewer & Stello 2009; Wang et al. 2012; Haywood et al. 2014; Ivezić et al. 2014; Rajpaul et al. 2015; Vanderburg et al. 2015; Luger et al. 2016; Foreman-Mackey et al. 2017; Karamanavis 2017; Chua et al. 2020; Jesus et al. 2020; Kovačević et al. 2019; Pereira et al. 2019; Wilkins 2019), and more generally in Bayesian signal estimation, is time series analysis based on Gaussian processes (GP; Rasmussen & Williams 2006; Roberts et al. 2012; Tobar et al. 2015; Durrande et al. 2016; Littlefair et al. 2017; Angus et al. 2018; Tobar 2018). GP analysis is intrinsically a Bayesian technique, i.e., prior information that encapsulates our assumptions on the analyzed time series (such as smoothness, stationarity, or periodicity) is adopted. Then, this is updated with the information provided by the observed data via a given likelihood function. Finally, a posterior distribution of the derived parameters can be used for any inference. GP are a generalization of multivariate Gaussian distributions of variables and offer a very flexible framework for modeling unknown functions by nonparametric models. A key component of the analysis is the kernel or covariance function. Given any arbitrary pair of observations, the kernel defines the degree of similarity between the observed values. There can be a plethora of possible kernel functions (squared-exponential, Matérn, etc.), although in practice, in most cases, just a few basic functions are used (Rasmussen & Williams 2006). Kernel functions drive the degree of smoothness of the observed light curves, and can also identify periodic behaviors and define an important connection between autoregressive time series methods and GP analysis (Rasmussen & Williams 2006; Durrande et al. 2016; Foreman-Mackey et al. 2017).

3. Methods

Our goal is to quantify the significance of possible periodicities in blazar light curves applying a procedure that allows us to draw inferences essentially independently of the sampling scheme of the analyzed (possibly multidimensional) data.

The choice of a specific covariance function can be often relatively arbitrary. A frequent choice, as in Angus et al. (2018), is the square exponential (SE) covariance function (Rasmussen & Williams 2006):

$$k_r = A \exp\left(-\frac{r^2}{2L^2}\right), \tag{1}$$

where $A > 0$ is the amplitude, L is the length scale of the exponential decay, and $r = (t_i - t_j)$ is the time separation between data points. This is a stationary kernel since it depends only on the data separation. The choice of the SE kernel is mainly driven by its simplicity, depending only on two parameters, A and L, although there are alternatives with the same number of parameters. In general, if L is large, the correlation between two data points largely separated will be stronger.

The SE kernel could be seen as a special case of the more general Matérn covariance function family (Rasmussen & Williams 2006; Durrande et al. 2016; Foreman-Mackey et al. 2017). The Matérn kernel functions are characterized by a parameter, ν, that drives the degree of "smoothness" of the kernel. Functions with $\nu = p - 1/2$ are the discrete time equivalent to AR (autoregressive) processes of order p. For $\nu \to +\infty$ the kernel becomes the SE covariance function while, with $\nu = \frac{1}{2}$, it simplifies to the absolute exponential (AE) kernel (i.e., the covariance of a Ornstein–Uhlenbeck

process):

$$k_r = A \exp\left(-\frac{r}{L}\right). \quad (2)$$

Finally, another interesting and frequently used stationary kernel is the rational quadratic (RQ) covariance function (Rasmussen & Williams 2006):

$$k_r = A\left[1 + \left(\frac{r^2}{2\alpha L^2}\right)^{-\alpha}\right], \quad (3)$$

with α strictly positive. This kernel can be seen as a scale mixture (i.e., an infinite sum) of SE covariance functions with different characteristic length scales drawn from a gamma distribution. The limit of the RQ covariance for $\alpha \to +\infty$ is indeed just the SE covariance function with characteristic length scale L.

In general, any covariance function mentioned above allows a satisfactory modeling of the data sets. However, having to deal with time series analysis requires some more care. The light curves considered in this work are characterized by a power spectral density (PSD) modeled by a power law (PL) or a broken PL (see Section 4 and, e.g., Nilsson et al. 2018; Covino et al. 2019) and therefore it is important that the adopted covariance functions provide an adequate description of the data and their PSDs. As reported by Wilkins (2019), the SE kernel does not correctly describe the PSD of the data, in particular at low frequencies. On the contrary, the AE and RQ kernels provide better results. The best choice depends on the specific PSD functional form. The multiple length-scale sensitivity of the RQ kernel makes it an interesting choice for blazar light curves, i.e., characterized by a complex variability pattern; however, the SE and AE kernels need a lower number of free parameters. We considered in our analyses both the AE and the RQ kernels, as discussed in Section 5.1.

Different families of kernels are needed to describe periodic behaviors. The simplest possibility is "the cosine" (CS) kernel:

$$k_r = A \cos(2\pi r/P), \quad (4)$$

where again $A > 0$ is the amplitude and r is the separation between data points. P is the period in the data. A more flexible and also widely used covariance function is the "exp-sine-squared" (ESS) kernel (Rasmussen & Williams 2006):

$$k_r = A \exp\left[-\Gamma^2 \sin^2\left(\frac{\pi r}{P}\right)\right], \quad (5)$$

where, if the additional parameter Γ is large, points separated by a period are strongly correlated, while the correlation is looser if Γ becomes small.

The ESS kernel offers a larger flexibility in modeling quasi-periodic phenomena, yet the CS kernel also allows negative covariances, a feature often present in the case of periodic behaviors and characterizing the autocorrelation functions of the data considered in this study (see Section 5.2).

The product or the sum of two (or more) kernel functions is still a legitimate kernel function (Rasmussen & Williams 2006). The sum and product of covariance functions reflect two different scenarios. A sum of two kernels gives higher values when the first "or" the second operands support high correlation, while for the product this occurs when the first "and" the second operands are both giving high correlation. In the following we report results both for the sum and the product and adopt a kernel derived by the combination of the AE or RQ and the CS covariance functions.

The problem of determining the possible presence of periodic behavior in a light curve can thus be converted to a plain model comparison in a Bayesian framework (e.g., Kass & Raftery 1995; Trotta 2008; Ivezić et al. 2014; Andreon & Weaver 2015), i.e., fitting the data with a stationary kernel and a more complex model with a periodic component. We also did not define any prior on the mean function, in order not to bias our results assuming a given functional form. The procedure we followed consists of initially maximizing the likelihood function by a nonlinear optimization algorithm (e.g., the Nelder-Mead or the L-BFGS-B algorithms, Gao & Han 2012; Byrd et al. 1995) and integrating the posterior probability density of the parameters of our models by a Markov Chain Monte Carlo (MCMC; Hogg & Foreman-Mackey 2018) based on the "affine-invariant Hamiltonian" and the "parallel-tempering ensemble" algorithms (Foreman-Mackey et al. 2013). We started the chains from small Gaussian balls centered on the best-fit values. The first third of each chain (the "burn-in phase") was discarded and we checked that a stationary distribution was reached (Sharma 2017). Model comparison could be carried out by evaluating the Bayesian information criterion (BIC; Schwarz 1978), which is simple to compute but requires that the posterior distribution of the parameters is essentially Gaussian, often an assumption not satisfied. We therefore carried out model comparison by a full computation of the Bayes factors (Ivezić et al. 2014), typically much more demanding computationally, but not requiring any special assumption (see also Liddle 2007). We computed the Bayes factors, following Littlefair et al. (2017), by the so-called "thermodynamic integration" (Goggans & Chi 2004), which indeed offers an effective compromise between accuracy and computational complexity.

The model comparison to assess whether the introduction of a periodic term is preferred compared to stationary covariance functions is then carried out leaving the GP regression free to identify possible periods (within a given large range) that can then be evaluated analyzing the posterior distribution of periods obtained after the analysis (Section 5).

Finally, the significance of the introduction of a periodic component in the modeling of the light curve typically has to be corrected for a trial factor, i.e., the number of independent frequencies that are "tried" (explicitly or implicitly) during the analysis. There is a large amount of literature about this topic. The number of independent frequencies depends on the length of the time series and on the sampling. This is not typically a problem with a simple solution, but approximate estimates are often adequate for most practical purposes (e.g., Horne & Baliunas 1986; Schwarzenberg-Czerny 1998; Cumming 2004; Baluev 2008; Frescura et al. 2008; Zechmeister & Kürster 2009; Baluev 2013; Süveges 2014).

However, the computation of the Bayes factor already includes the multitrial correction, since it is embedded in the integration on the allowed parameter space defined by the priors on the analysis (e.g., Gelman & Tuerlinckx 2000; Trotta 2007; Gelman et al. 2012). Effectively, the Bayes factor model selection takes into proper account all the information provided by the data.

Software tools and packages used throughout the present analyses are listed in Appendix B.

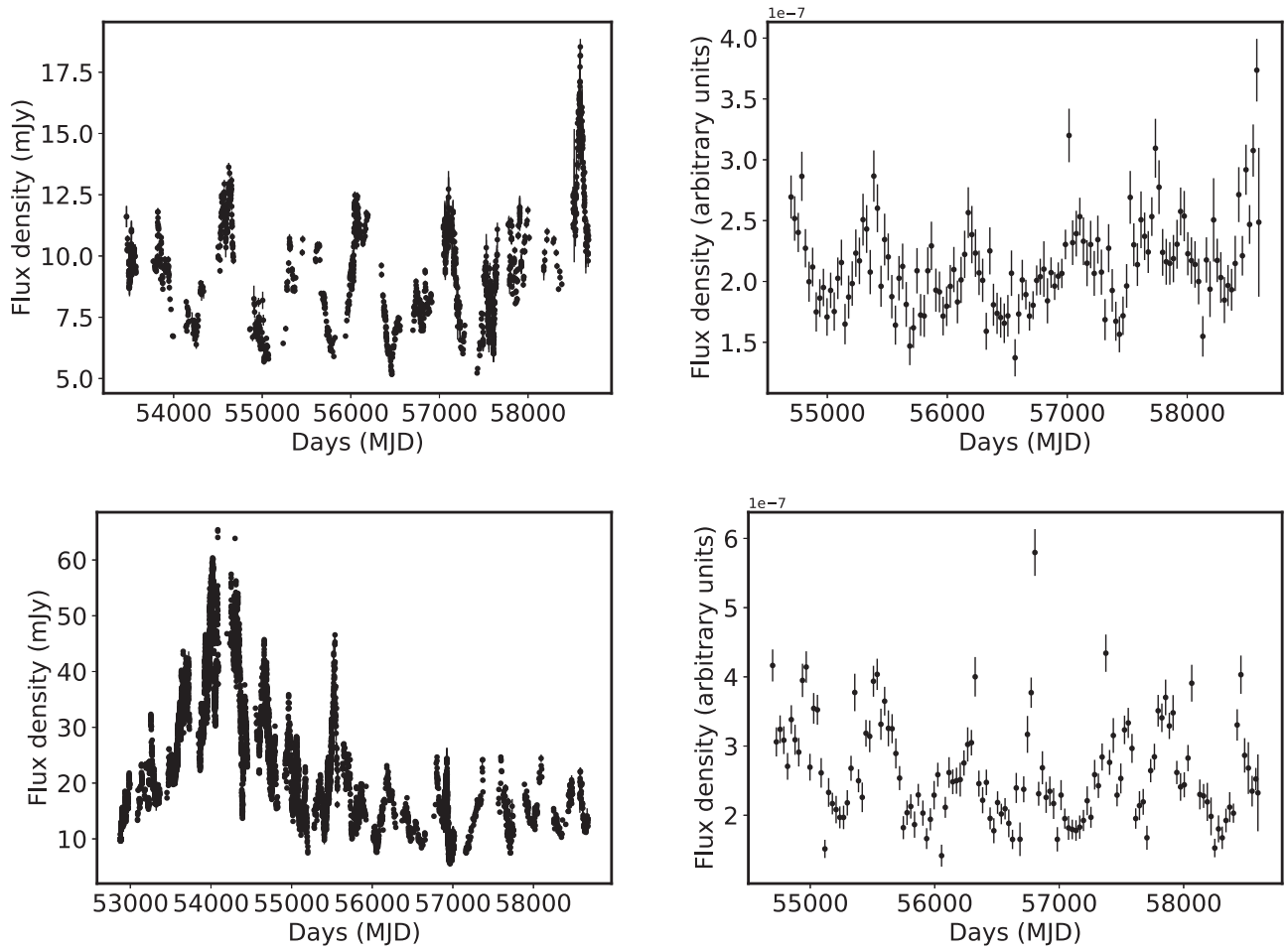

Figure 1. Optical (*R*-band, left column) and high-energy (100 MeV to 200 GeV, right column) light curves for the blazars considered in this study. From top to bottom, PG 1553 + 113 and PKS 2155–304, respectively. The optical data are shown here with the original sampling, while for the periodicity analysis they are binned at 30 days, analogously to the high-energy data.

4. Data

We selected two BL Lac objects based on the availability of well sampled optical light curves, Fermi high-energy data, and claims proposed in recent literature for possible periodicities (Section 1). The sources are PG 1553+113, at a redshift of $z \gtrsim 0.30$ (Landoni et al. 2014), and PKS 2155–304, at a redshift $z \sim 0.12$ (Falomo et al. 1991).

The optical data (*R*-band) are from several different telescopes and were already discussed in Sandrinelli et al. (2014, 2016a, 2018). Additional optical data covering the more recent epochs are reported in Appendix A. We refer the reader to the quoted papers for all the details about data reduction and analysis. The 100 MeV to 200 GeV Fermi data have been updated with the latest observations discussed in Covino et al. (2019). Given that we are mainly interested in rather long (several months) possible periodicites, optical and high-energy data are binned with a 30 day sampling. These data sets cover more than a decade of observations for all the sources considered in this work. Fermi data are regularly sampled, while optical data present gaps due to seasonal visibility or other problems affecting the observations (Figure 1).

For PG 1553 + 113, a period of $T \sim 796$ days analyzing the Fermi/LAT light curve was proposed by Ackermann et al. (2015) and the same period was reported to be consistent with data in other bands (e.g., Cutini et al. 2016; Stamerra et al. 2016). With a longer coverage the periodicity in the Fermi data was confirmed by Tavani et al. (2018). A consistent periodicity in the optical data, together with a confirmation at high energies, was discussed by Sandrinelli et al. (2018).

For PKS 2155–304, in the optical, a periodic component at slightly less than one year, superposed on a long-term trend with large-amplitude variations, was proposed by Zhang et al. (2014). The same period ($T \sim 315$ days) was found by Sandrinelli et al. (2014), while a period of approximately two times the optical one ($T \sim 642$ days) was identified analyzing the Fermi/LAT light curve (see also Sandrinelli et al. 2016a). Confirmation of the periodicity at high energies with longer coverage by the Fermi satellite was proposed by Zhang et al. (2017b). A reanalysis of more recent data in the optical and high-energy by Sandrinelli et al. (2018) confirmed the previous findings.

These periods for both sources were also identified in the Fermi/LAT data by the systematic search carried out by Prokhorov & Moraghan (2017), while Covino et al. (2019) and Ait Benkhali et al. (2020) shed some doubt on the claimed significance of the proposed periodicities at high energy for these two sources (and other blazars observed by Fermi). Nilsson et al. (2018) also did not find any evidence for periodicity in the optical data of both sources (and other blazars were well observed in the optical).

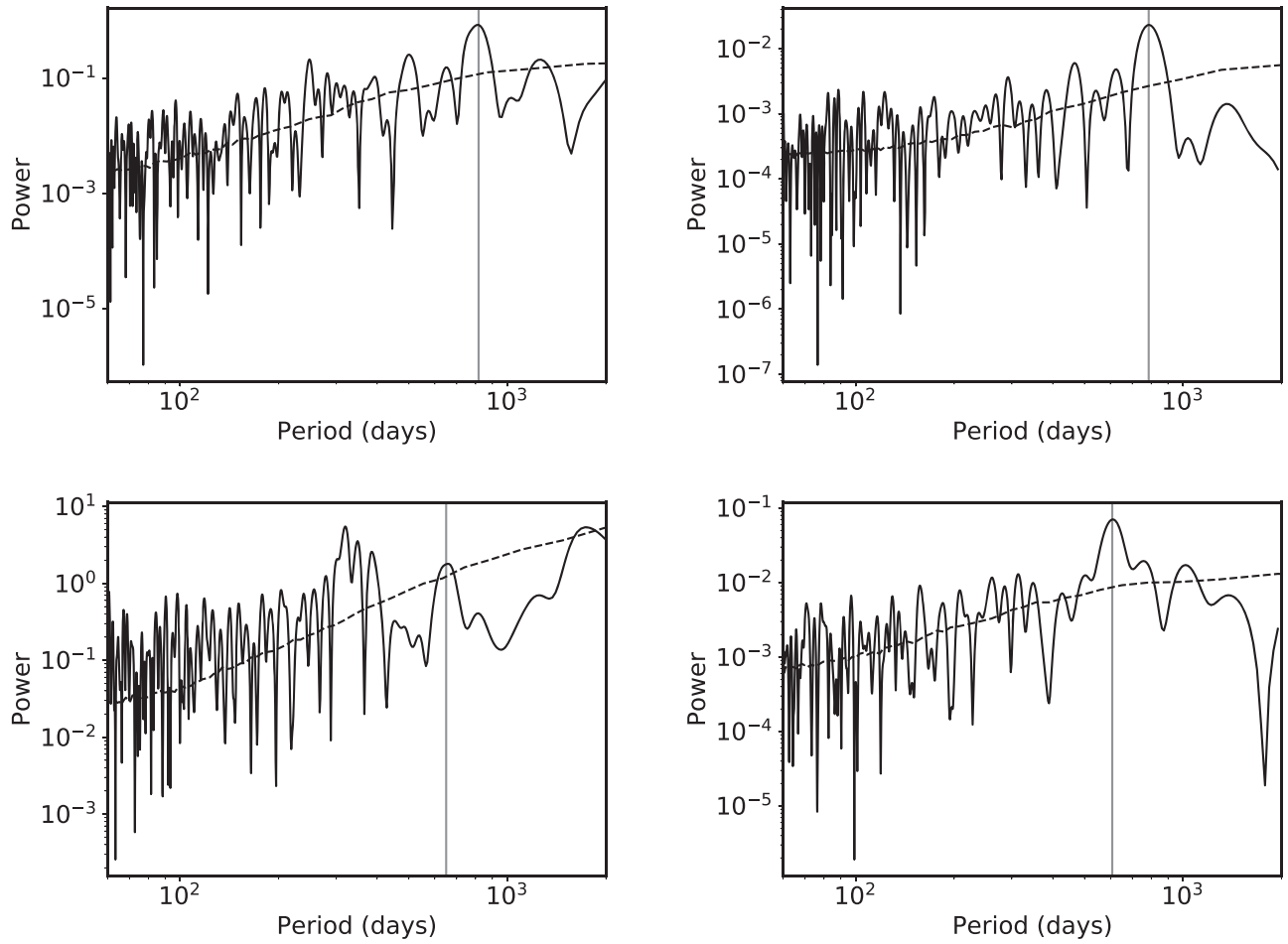

Figure 2. Optical (*R*-band, left column) and high-energy (100 MeV to 200 GeV, right column) Lomb–Scargle periodograms based on the light curves of the blazars considered in this study. From the top to the bottom, PG 1553 + 113 and PKS 2155–304, respectively. The vertical lines indicate the most prominent periods identified in the periodograms (Table 1). The dashed lines are the PSD for the best-fit AE kernel (see Sections 3 and 5.1).

5. Results

The light curves for the two objects of our interest (Figure 1) show intense variability, as is typical for this category of sources (e.g., Lindfors et al. 2016). The high-energy and optical monitoring both cover more than a decade of observations, therefore allowing us to explore at least a few cycles for year-long periodicities. We first checked whether our light curves are consistent with standard stationarity tests, i.e., the Augmented Dickey-Fuller unit root test (ADF) and the Kwiatkowski–Phillips–Schmidt–Shin (KPSS) test (e.g., Kwiatkowski et al. 1992; Hamilton 1994). These tests show that, to some extent, for all light curves but the high-energy data of PKS 2155–304, nonstationarity is present, as is easy to infer even after a visual inspection (Figure 1) due to the presence of large flares. At variance with other analysis techniques, GP regression, however, does not typically require one to assume stationarity of the light curves (Kovačević et al. 2019) for deriving reliable inferences.

We then carried out a period analysis by means of a generalized LS algorithm (Lomb 1976; Scargle 1982; Bretthorst 2003; VanderPlas 2018). The derived periodograms are shown in Figure 2 and their maxima are also identified (Table 1). The PKS 2155–304 LS periodogram (Figure 2) does not show a prominent peak, at variance with the other cases here considered. A relatively isolated peak is indeed visible at ∼650 days, close to the high-energy period. Therefore, following Chevalier et al. (2019), who also considered a periodicity in the optical consistent with the high-energy one, and driven by the intrinsic interest of possible synchronous periodicities in different bands, we report $P \sim 650$ days in Figure 2 and Table 1.

Table 1
Periods Corresponding to the Maximum Power Detected in the Lomb–Scargle Periodograms Shown in Figure 2

Source	Optical Period (days)	High-energy Period (days)
PG 1553 + 113	820	790
PKS 2155–304	650	610

Note. The optical and high-energy light curves give consistent periods for PG 1503+113. For PKS 2155–304, in the optical, we chose to show a period similar to the high-energy one even if a single dominant feature cannot be easily identified (see Section 4).

It is also apparent that for both sources the periodograms are characterized by noise increasing toward long periods, the typical behavior when noise is correlated (Press 1978; Milotti 2002, 2007). Modeling the noise as power laws, their indices were previously evaluated in the literature (Nilsson et al. 2018; Covino et al. 2019) and they are approximately in the range of 1–1.5. Given that the proposed periodicities are all close to the low-frequency tail of the derived periodograms, any evaluation of their significance must therefore be carried

Table 2
Bayes Factors for the High-energy (HE) and the Optical (Opt) Light Curves and the Associated Probabilities Conditioned on the Data of Supporting One Model (e.g., RQ or AE) over Another (SE or RQ)

Source	Band	BF_{SE-RQ}	BF_{SE-AE}	BF_{RQ-AE}
PG 1553 + 113	HE	14 ± 2	85 ± 6	6 ± 1
	Opt	>1000	>1000	4 ± 1
PKS 2155–304	HE	71 ± 10	445 ± 28	6 ± 1
	Opt	>1000	>1000	4 ± 1

Note. Their 1σ credible regions are also reported. Flat uninformative or Jeffrey priors on the parameters were added to the likelihood function.

out with great care (see Section 2 and the discussion in Bhatta & Dhital 2020).

5.1. Stationary Kernels

For all the light curves considered in this study, we could obtain reasonable fits by GPs with any of the kernel discussed in Section 3. This is not surprising, given the flexibility provided by GP regression, as widely discussed in the literature (Ivezić et al. 2014; Foreman-Mackey et al. 2017; Littlefair et al. 2017; Angus et al. 2018). As mentioned in Section 3, the AE and the RQ kernels are, however, better suited to model our blazar light curves. Together with the considerations discussed in Wilkins (2019), the choice is also supported by more formal arguments, since both the RQ and the AE kernel functions are preferred over the simpler SE kernel based upon a Bayesian model comparison. In turn, the AE kernel is only moderately preferred over the RQ kernel, and for the next steps of our analysis we considered both the possibilities. In Table 2 we report the computed Bayes factors. The large uninformative priors adopted in the analysis are reported in Appendix C.

If the posterior probabilities of two competing models, e.g., models "0" and "1", are, respectively, p_0 and p_1, Bayes factors can be easily converted to probabilities conditioned on the data in favor of model "1" with respect to model "0" as (e.g., Trotta 2007):

$$p = p_1/(p_0 + p_1) = BF_{0-1}/(BF_{0-1} + 1), \quad (6)$$

where $BF_{0-1} = p_0/p_1$. Therefore, BF ~ 1 means $p \sim 50\%$, BF ~ 10 is slightly larger than $p \sim 90\%$ and BF ~ 100 gives $p \sim 99\%$.

For stationary kernels, covariance functions and PSDs are Fourier duals (Rasmussen & Williams 2006), and in Figure 2 we also show the PSD derived by the AE kernel with the best-fit parameters reported in Appendix D.

The best-fit values of the parameters (also often called "hyperparameters") of the kernel functions are not, in general, of straightforward interpretation. The relatively large values for the correlation length parameter L, for the AE kernel and the low values of the `gamma` distribution parameter "α" for the RQ kernel (Appendix D) imply a correlation slowly decaying with increasing data separation (Rasmussen & Williams 2006). This is in qualitative agreement with the long-term noise correlation singled out by modeling periodograms for these sources, as, e.g., in Nilsson et al. (2018) and Covino et al. (2019).

5.2. Periodic Kernels

Adding a periodic component to the kernel function increases the complexity of the analysis and of course the capability of the model to reproduce the data and the associated noise. In the present work, we leave the kernel parameters essentially unconstrained with uninformative large flat or Jeffrey priors (see Appendix C). The periods, in particular, are constrained to be within a large (100–2000 day) flat range (see, e.g., Kass & Raftery 1995; Trotta 2008, for a discussion about prior role in Bayesian model comparison). All the adopted priors are properly normalized in order that the obtained posterior distributions are actual probability distributions (e.g., Tak et al. 2018).

We have explored all the combinations of the AE and RQ kernels with the periodic CS kernel, namely AE $\times$ CS, RQ $\times$ CS, AE+CS, and RQ+CS, listed with increasing number of free parameters (3, 4, 4, and 5, respectively). Covariance functions including a periodic component typically yield similar results, i.e., better posterior probabilities, compared to the stationary kernel description only, as measured by the computed Bayes factors (Table 3). The preference for the description including a periodicity is partly expected basing on the results of the LS analysis and also because the two sources here considered were selected for the relevance of past periodicity studies. The AE $\times$ CS combination turns out to be too simple, since the rapid decay of the covariance described by the AE kernel for separations larger than a few times the correlation length make the multiplied periodic kernel essentially ineffective. This is not the case for the RQ kernel since its greater flexibility allows it to model correlation on longer scales.

Results of the stationary versus period kernel analysis show that there is a rather solid preference for a modeling requiring a period component for PG 1553 + 113, both at high energies and in the optical. On the contrary, for PKS 2155–304, the preference for a periodic component is weaker at high energy and not supported by the data in the optical.

In Figure 3 a random selection of possible solutions, with the RQ $\times$ CS kernel, extracted for the posterior distribution of the parameters is shown superposed to the original light curves.

Even if the addition of a kernel with a periodic component is favored by the data, it is still worth checking the obtained solutions in order to reach a better insight about the meaning of the GP regression results. To this aim, in Figure 4, we plot the autocorrelation functions (ACF) and the best-fit based on the RQ $\times$ CS kernel function. It is clear that for PG 1553 + 113 and for the high-energy data of PKS 2155–304 the periodic kernel shows correlation peaks at the derived periods and the adopted covariance function correctly describes the ACF computed on the real data. Clearly, reality is richer than our models and peaks in the ACF never repeat identically, while our models do. However, the average amplitude of the oscillations characterizing the ACFs for PG 1553 + 113 is larger than that for PKS 2155–304, suggesting the main reason for the lower Bayes factor obtained for the latter source. The case of the optical data of PKS 2155–304 looks different, with no evidence for an actual periodicity in the data.

A different procedure for evaluating the importance of the addition of a periodic component in the analysis is possible when covariance functions obtained by the sum of a stationary and a periodic kernel are applied (in the present study, AE+CS

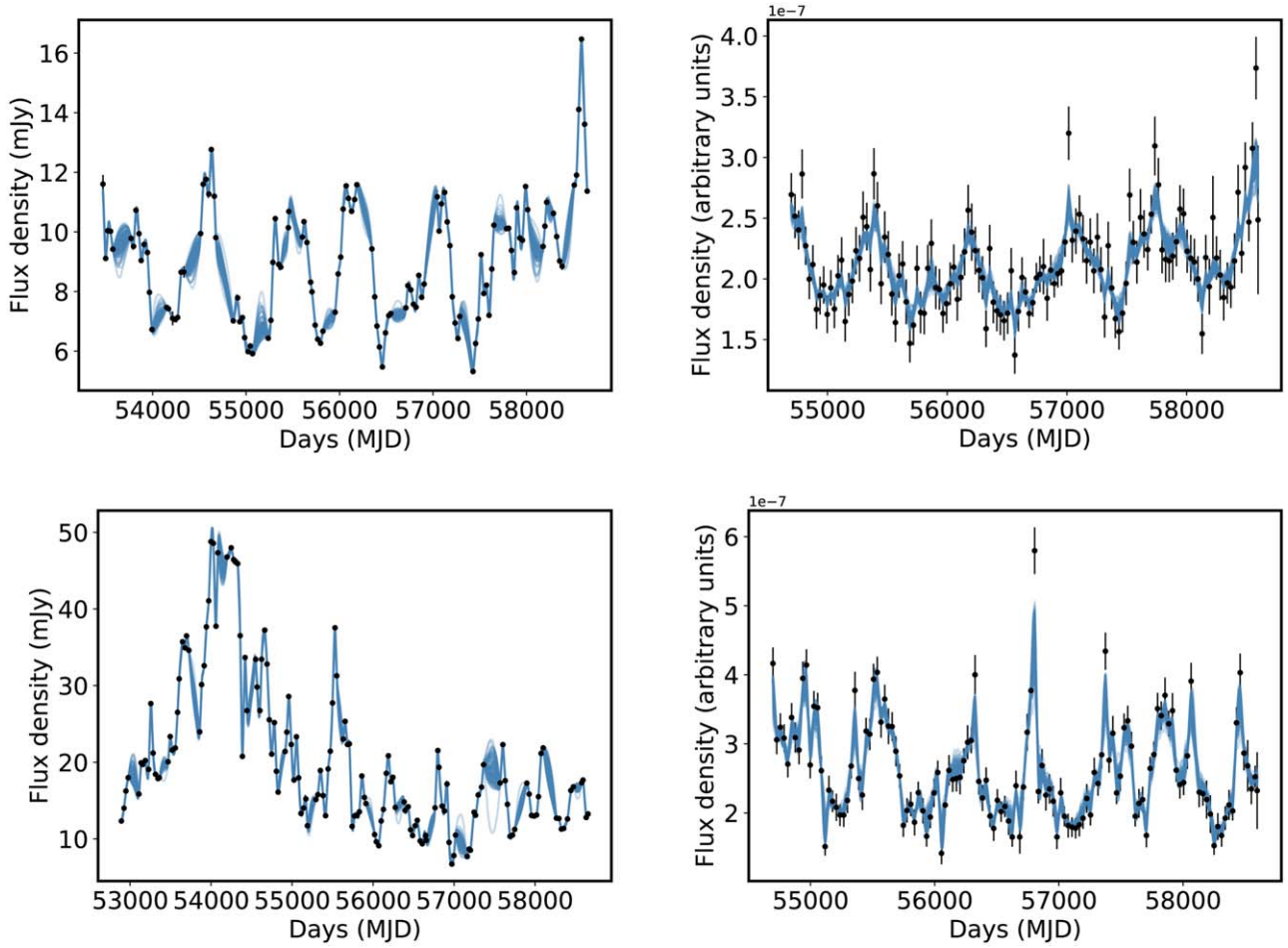

Figure 3. Fit to the light curve based on a GP regression with a RQ × CS periodic kernel. Superposed to the light curve, a sample of 100 random sets of parameters drawn for the posterior distribution is plotted. Optical data (*R*-band, left column) and high-energy data (100 MeV to 200 GeV, right column). From the top to the bottom, PG 1553 + 113 and PKS 2155–304, respectively. The optical data are binned with 30 day sampling analogously to the high-energy data.

Table 3
Bayes Factors for the High-energy (HE) and the Optical (Opt) Light Curves for the various Combinations of Stationary and Period Kernels Considered in This Study

Source	Band	$BF_{AE-(AE\times CS)}$	$BF_{RQ-(RQ\times CS)}$	$BF_{AE-(AE+CS)}$	$BF_{RQ-(RQ+CS)}$
PG 1553 + 113	HE	2.0 ± 0.2	202 ± 40	223 ± 53	1709 ± 410
	Opt	7.2 ± 0.7	261 ± 51	115 ± 35	866 ± 222
PKS 2155–304	HE	1.0 ± 0.1	50 ± 11	5 ± 1	27 ± 12
	Opt	≪1	≪1	1.3 ± 0.2	1.0 ± 0.2

Note. The 1σ credible regions for the computed Bayes factors are also reported. Flat uninformative or Jeffrey priors on the parameters were added to the likelihood function.

or RQ+CS). An estimate of the role of the periodic component can be derived by the analysis of the variance associated to the latter component with respect to the former (the A_{AE}, A_{RQ}, and A_{CS} parameters in Appendix D), and the marginalized posterior distribution of the variance associated to the periodic kernel. First of all, from the various fit results reported in Appendix D, we see that for the high energy data of PG 1553 + 113 the variance associated to the CS kernel is only slightly lower than the one associated to AE or RQ kernels, while for the optical data the periodic kernel describes only a minor fraction of the variance associated to the stationary kernel. In general, however, the model with the RQ kernel provides more constrained parameters although, for PKS 2155–304, the variance associated to the CS kernel is always badly defined. The variance associated to the CS kernel for PG 1553 + 113 is greater than zero with high confidence (better than 99.97% level) at high energies and at a lower yet high level (98%) in the optical. For PKS 2155–304, the null hypothesis of zero variance associated to the periodic kernel cannot be ruled out even at a much lower confidence level.

Finally, we show the marginalized posterior distribution for the periods (Figure 5) for the RQ+CS covariance function. This also allows us to investigate the capabilities of a composite periodic kernel function to identify periodicities. The main peaks identified by the LS analysis (Figure 2) are visible, and the adopted periodicities in the analysis are confirmed. No other periods are singled out, and the distributions are clearly single-peaked with most of the

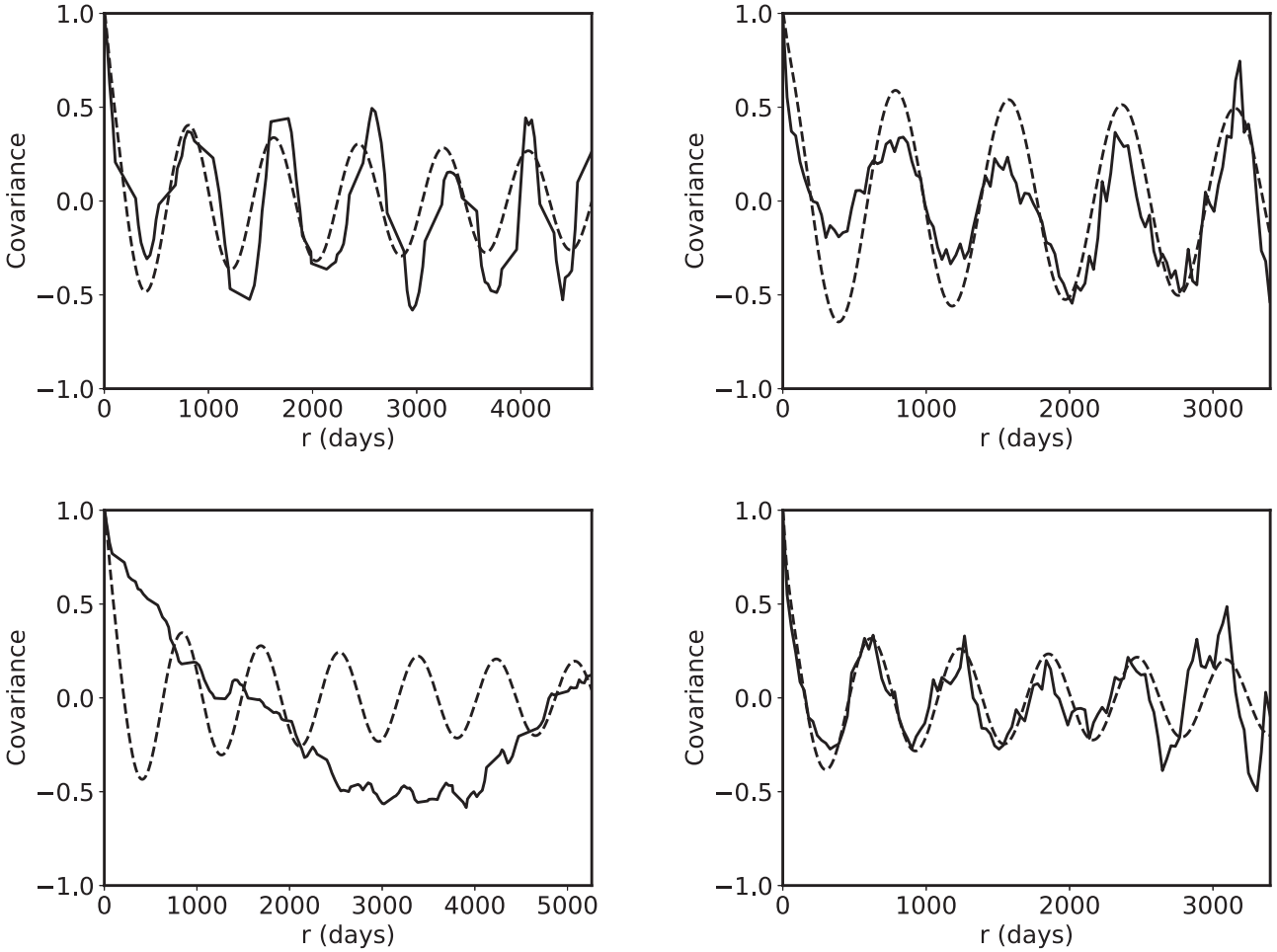

Figure 4. Plot of the best-fit RQ × CS kernel functions together with the ACF computed from the data. The quantity in abscissa, $r = (t_i - t_j)$, is the separation between data points. Optical data (*R*-band, left column) and high-energy data (100 MeV to 200 GeV, right column). From the top to the bottom, PG 1553 + 113 and PKS 2155–304, respectively. The dashed line is for the best-fit kernel and the solid line is for the ACF.

posterior probabilities lying around the identified periods. Again, PKS 2155–304 in the optical is an exception, and no period stands out for this source, although minor peaks can easily be singled out.

5.3. Comparison with Past Results

We have selected high energy and optical data for two blazar sources with several different claims of possible QPO in the literature (see Section 4). Summarizing, in our work we find rather solid evidence supporting the presence of an ∼2.2 year QPO for PG 1553 + 113, while for PKS 2155–304 the evidence is weaker and still inconclusive at high energies, or there is no evidence at all in the optical. The QPO in PG 1553 + 113 was first reported by Ackermann et al. (2015) and later confirmed by Tavani et al. (2018), while Covino et al. (2019) and Ait Benkhali et al. (2020) did not find evidence for it. For PKS 2155–304, a year-long period in the optical was suggested by Zhang et al. (2014) and a hint for a periodicity at high energy, approximately two times longer than the optical one, was suggested by Sandrinelli et al. (2016a). No periodicities in the optical for both sources emerged from the analyses by Nilsson et al. (2018).

It is therefore of interest to see the reasons for these partially (possibly apparently) contradictory results. In general, reporting a possible periodicity always depends on the comparison between a null hypothesis, i.e., the light curve is pure noise, and a hypothesis implying a periodic behavior. Independently of the specific analysis technique applied, any inference is driven by the capability to correctly interpret and model the noise of the data under analysis and by the capability to identify periodic behaviors. These are not trivial tasks and often remain inadequately discussed. The noise is typically modeled, implicitly or explicitly, as PLs or broken PLs. Then, an excess power at a given frequency is compared to the prediction of the pure noise model. The power can be measured by two general sets of techniques: parametric and nonparametric. The first class includes the Fourier transform (as in Covino et al. 2019) or the popular LS algorithm (as in Nilsson et al. 2018). These parametric techniques require one to model a light curve by a harmonic decomposition, which can be ineffective in identifying even real periods in cases of very noisy data and covering only a few cycles of the search for periodicity (see also the discussion in Bhatta & Dhital 2020), as is the case of the data considered here. On the other hand, nonparametric techniques (as in Ackermann et al. 2015; Tavani et al. 2018, and for our GP analysis) do not require one to describe the data with a given functional form and might be better suited to extract hidden periodic signals in very noisy data. A full discussion of the pros and cons of parametric and nonparametric time-series analysis techniques is certainly beyond the goal of the present study. Yet, we think it is plausible that some of the different claims we mentioned are simply due to difference

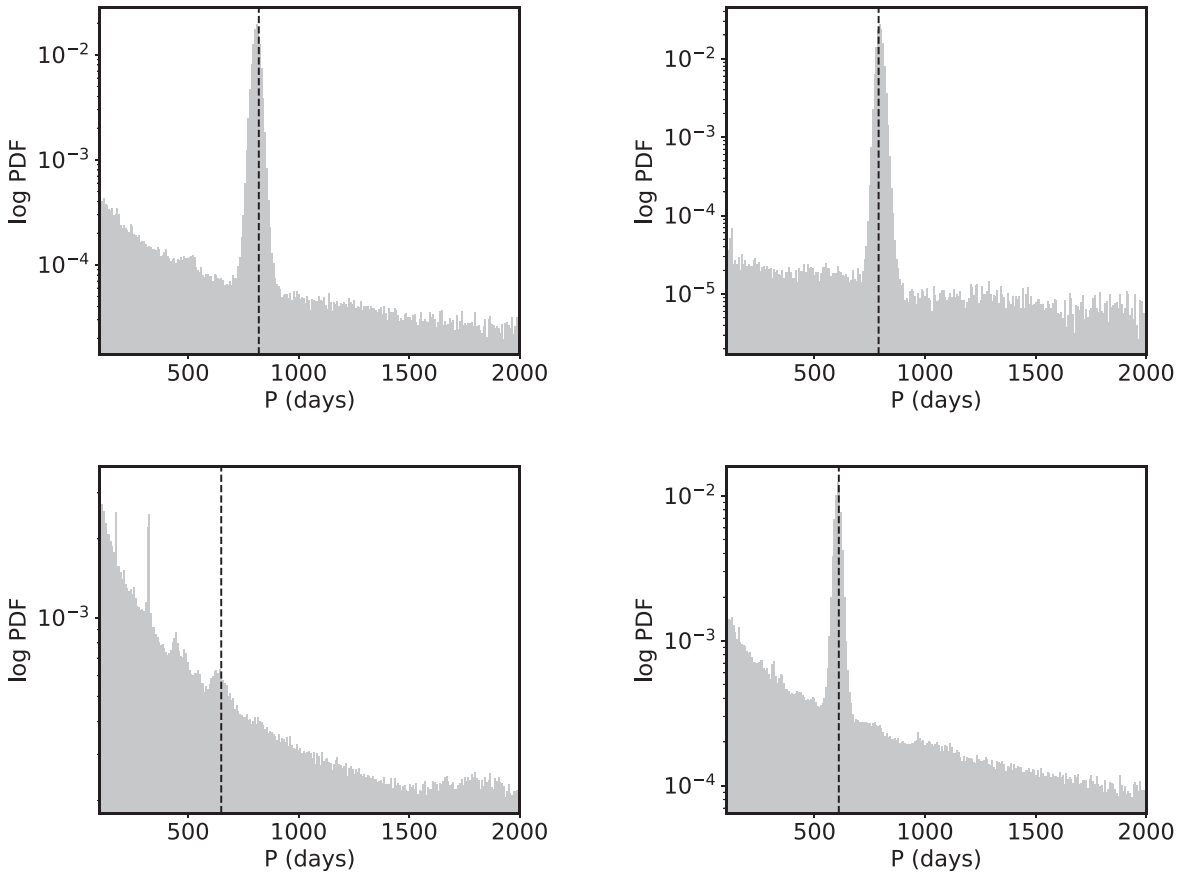

Figure 5. Marginalized posterior probability density functions for the periods singled out with the RQ+CS covariance function (results with other kernel functions are very similar). The PDF are derived by a GP regression and a flat prior from 100 to 2000 days for the optical data (*R*-band, left column) and high-energy data (100 MeV to 200 GeV, right column). From the top to the bottom, PG 1553 + 113 and PKS 2155–304, respectively. The vertical lines indicate the periods identified by the LS analysis (Figure 2).

in the data analysis emphasized by the short coverage, in terms of number of cycles, of the available data.

6. Conclusions

In this work we addressed the problem of assessing the significance of periodicities proposed in the literature for two of the most studied blazars: PG 1553+114 and PKS 2155–304. We made use of high-energy data, from the Fermi/LAT instrument, and optical data collected by several telescopes. These data have partly already been analyzed in previous papers (see Section 4). The whole topic of blazar year-long possible periodicities is widely discussed in the literature with several papers reporting even contradicting results (see, e.g., Rieger 2019, for a recent discussion). Our approach is based on GP regression that, in spite of being computationally relatively demanding, offers several advantages. The analysis does not need to be carried out in the frequency space, with all the possible problems induced by irregular sampling, gaps, etc. The inference relies on a Bayesian model comparison between two possible hypotheses: one only able to describe the correlated noise affecting blazar light curves, and another with an addition of a periodic component left free to vary in the range of interest. No assumption about the form of the possible periodic variation was included in the analysis although, in the presence of physically motivated scenarios, this could be done.

Our results, summarized in Tables 2 and 3, show that the addition of a periodic component always improve the description of the data, in substantial agreement with the various results in the literature. For PG 1553 + 113 the improvement seems to be relatively solid both at high energies and in the optical, while for PKS 2155-305 the situation is still inconclusive at high energies and no periodicity seems to be present in the optical.

This is at present mainly an exploratory study. Many aspects of a GP-based analysis need to be more deeply evaluated in future works. One of the most critical topics is about the choice of the covariance functions (Wilkins 2019) or the criteria for selecting the best among different possible combinations (e.g., Duvenaud et al. 2013). The problem does not have a simple solution. Time series analyses require a modeling of the light curves and of their PSDs. We have here limited our study to the most commonly used kernel functions for GP analysis (Rasmussen & Williams 2006), but the subject is receiving increasing attention in the literature (e.g., Wilson & Prescott Adams 2013; Durrande et al. 2016; Foreman-Mackey et al. 2017; Tobar 2018).

Another interesting topic is related to the possibility to run a GP regression with multidimensional input data, therefore, providing a natural environment to study time series available in multiple bands. The analysis can be carried out with different kernel functions in different bands, if needed, and adding a periodic kernel with the same periods for all the input data. This will allow us to optimally use all available information for statistical inference.

We thank the anonymous referee for a rich and inspiring report. S.C. is grateful to Dr. Luigi Stella and Dr. Stefano Andreon for very profitable discussions, and to Dr. Ben Granett for having carefully read the manuscript. We acknowledge

partial funding from Agenzia Spaziale Italiana-Istituto Nazionale di Astrofisica grant I/004/11/3.

Appendix A
Optical Data

The optical data for PG 1553 + 113 and PKS 2155–304 analyzed in this work were partly published in Sandrinelli et al. (2014, 2016a, 2018). Here we report data obtained after the publication to the present epoch. We refer to the quoted publications for all the details about data reduction and analysis.

Tables A1 and A2, contain data for PG 1553 + 113 and PKS 2155–304, respectively. For both tables, Column 1 lists the MJD of the observation, Column 2 gives the R_c magnitude and Column 3 its 1σ error.

We refer the reader to the reported references for anything related to data reduction, analysis, and calibration.

Table A1
Optical Data for PG 1553 + 113

MJD (Days)	Magnitudes (R_c band)	1σ Error
53468.40516	13.57	0.03
53495.11636	13.76	0.03
53499.10951	13.88	0.01
53501.12239	13.88	0.01
53503.10500	13.82	0.01
53506.13048	13.80	0.01
53511.17848	13.81	0.01
53518.05972	13.75	0.01
53523.03968	13.68	0.02
53526.03937	13.74	0.02
53528.03765	13.81	0.03
53538.13407	13.76	0.00
53556.10483	13.71	0.00
53573.03119	13.78	0.01
53970.04372	14.00	0.01
53995.98658	14.16	0.01
54218.26792	14.14	0.05
54234.33117	14.09	0.05
54255.12331	14.22	0.03
54331.02096	13.88	0.03
54574.25162	13.59	0.05
54588.38112	13.63	0.10
54906.38731	13.94	0.07
54921.35537	14.09	0.03
54935.38222	14.13	0.06
54950.31922	14.08	0.03
54966.27467	14.04	0.03
54982.33886	14.23	0.03
55005.27961	13.95	0.05
55028.21905	14.31	0.03
55982.37299	13.97	0.07
56011.21562	13.89	0.02
56013.24880	13.87	0.02
56016.39511	13.79	0.02
56019.32278	13.79	0.01
56021.33930	13.76	0.01
56026.22237	13.82	0.03
56029.23440	13.83	0.01
56034.21658	13.76	0.02
56036.34757	13.63	0.02
56042.22173	13.63	0.02
56047.22496	13.59	0.03
56062.35472	13.53	0.03
56065.18069	13.66	0.02
56067.36846	13.68	0.02

Note. Column 1 lists the MJD of the observation, column 2 gives the R_c magnitude, and column 3 gives its 1σ error.

Table A2
Optical Data for PKS 2155–304

MJD (Days)	Magnitude (R_c band)	1σ Error
55516.04326	12.36	0.04
55518.11836	12.51	0.05
55521.02647	12.30	0.05
55523.04867	12.20	0.03
55525.14933	12.26	0.04
55531.10888	12.41	0.04
55533.13191	12.23	0.04
55536.13616	12.11	0.04
55538.11141	12.22	0.04
55540.08721	12.44	0.04
55542.08486	12.41	0.04
55544.06030	12.38	0.04
55547.10680	12.51	0.05
55552.04550	12.59	0.05
55559.08028	12.77	0.04
55562.06174	12.70	0.04
55565.04775	12.82	0.04
55567.06705	13.02	0.03
55571.05565	12.99	0.04

Note. Column 1 lists the MJD of the Observation, column 2 gives the R_c magnitude, and column 3 gives its 1σ error.

Appendix B
Software Packages

We have developed software tools and used third-party libraries all developed with the `python` language (van Rossum 1995) (v. 3.7)[3] with the usual set of scientific libraries `numpy` (Oliphant 2006) (v. 1.15.4)[4] and `scipy` (Jones et al. 2001) (v. 1.10).[5] The ADF and KPSS stationarity tests are coded in the `statsmodels` library (v. 0.9.0).[6] The generalized LS algorithm we applied is part of the `astropy` (v. 3.1.2)[7] suite (Astropy Collaboration et al. 2013, 2018). ACF are computed by `numpy` tools. Nonlinear optimization algorithms and numerical integration tools are provided by the `minimize` and `integrate` subpackages of the `scipy` library. MCMC algorithms are provided by the `emcee`[8] (v. 2.2.1) library (Foreman-Mackey et al. 2013). GP analysis is carried out by the `george` package (v. 0.3.1)[9] (Ambikasaran et al. 2015). Plots are produced within the `matplotlib` (Hunter 2007) (v. 3.0.2)[10] framework. Multidimensional projection plots were obtained with the `corner` (Foreman-Mackey 2016) (v. 2.0.2)[11] library.

Table C1
Prior Information Adopted for for Analyses Described in Section 5

Hyperparameter	Prior
$\ln A$	Uniform [−20, 20]
$\ln L$	Uniform [−20, 20]
$\ln \alpha$	Uniform [−10, 10]
P	Uniform [100, 2000]

Note. P_0 is the period singled out by the LS analysis. All the priors are properly normalized for the computation of the Bayes factors.

Appendix C
Priors Imposed to the Analysis

Throughout this paper we have always adopted larger uninformative or Jeffrey priors (Table C1).

[3] http://www.python.org
[4] http://www.numpy.org
[5] https://www.scipy.org
[6] https://www.statsmodels.org/stable/index.html
[7] http://www.astropy.org
[8] http://dfm.io/emcee/current/
[9] https://george.readthedocs.io/en/latest/
[10] https://www.matplotlib.org
[11] https://corner.readthedocs.io/en/latest/

Appendix D
Best-fit Hyperparameters

We report here the best-fit hyperparameters obtained fitting our data with the SE kernel (Table D1), the AE kernel (Table D2), the RQ kernel (Table D3), the AE × CS kernel (Table D4), the RQ × CS kernel (Table D5), the AE+CS kernel (Table D6), and the RQ+CS kernel (Table D7). For our analyses, we have multiplied the high energy and the optical data by factors 10^7 and 10^3, respectively, for better numerical optimization. This has of course no effect on the reported results.

Table D1
1σ Credible Regions and the Maximum a Posterior Estimator for the Hyperparameters Derived by the Analysis Adopting the SE Kernel for the High-energy (HE) and the Optical (Opt) Light Curves

Source	Band	$\ln A$	$\ln L$
PG 1553 + 113	HE	$-2.46^{+0.29}_{-0.26}$	$4.44^{+0.25}_{-0.39}$
	Opt	$1.17^{+0.14}_{-0.14}$	$3.42^{+0.04}_{-0.04}$
PKS 2155–304	HE	$-0.85^{+0.15}_{-0.14}$	$4.31^{+0.07}_{-0.07}$
	Opt	$4.36^{+0.13}_{-0.12}$	$3.46^{+0.03}_{-0.03}$

Note. Flat uninformative or Jeffrey priors on the parameters were added to the likelihood function.

Table D2
1σ Credible Regions and the Maximum a Posterior Estimator for the Hyperparameters Derived by the Analysis Adopting the AE Kernel for the High-energy (HE) and the Optical (Opt) Light Curves

Source	Band	$\ln A$	$\ln L$
PG 1553 + 113	HE	$-2.14^{+0.51}_{-0.32}$	$5.24^{+0.65}_{-0.43}$
	Opt	$1.41^{+0.32}_{-0.24}$	$5.26^{+0.36}_{-0.27}$
PKS 2155–304	HE	$-0.73^{+0.22}_{-0.19}$	$4.31^{+0.28}_{-0.24}$
	Opt	$4.68^{+0.42}_{-0.29}$	$5.82^{+0.44}_{-0.31}$

Note. Flat uninformative or Jeffrey priors on the parameters were added to the likelihood function.

Table D3
1σ Credible Regions and the Maximum a Posterior Estimator for the Hyperparameters Derived by the Analysis Adopting the RQ Kernel for the High-energy (HE) and the Optical (Opt) Light Curves

Source	Band	$\ln A$	$\ln \alpha$	$\ln L$
PG 1553 + 113	HE	$-1.99^{+1.41}_{-0.47}$	$-1.45^{+1.36}_{-1.97}$	$4.11^{+0.64}_{-0.41}$
	Opt	$1.83^{+1.45}_{-0.48}$	$-1.85^{+0.85}_{-1.78}$	$3.97^{+0.70}_{-0.25}$
PKS 2155–304	HE	$-0.63^{+0.72}_{-0.24}$	$-1.00^{+0.75}_{-1.41}$	$3.28^{+0.25}_{-0.20}$
	Opt	$6.00^{+1.89}_{-1.04}$	$-3.92^{+1.19}_{-1.95}$	$4.53^{+0.94}_{-0.51}$

Note. Flat uninformative or Jeffrey priors on the parameters were added to the likelihood function.

Table D4
1σ Credible Regions and the Maximum a Posterior Estimator for the Hyperparameters Derived by the Analysis Adopting the AE × CS Kernel for the High-energy (HE) and the Optical (Opt) Light Curves

Source	Band	$\ln A$	$\ln L$	$\ln P$
PG 1553 + 113	HE	$-2.18^{+0.44}_{-0.33}$	$5.58^{+0.67}_{-0.52}$	$6.95^{+0.38}_{-0.28}$
	Opt	$1.42^{+0.28}_{-0.23}$	$5.43^{+0.32}_{-0.28}$	$6.92^{+0.35}_{-0.25}$
PKS 2155–304	HE	$-0.74^{+0.22}_{-0.19}$	$4.39^{+0.30}_{-0.27}$	$6.89^{+0.47}_{-0.47}$
	Opt	$4.55^{+0.31}_{-0.24}$	$5.68^{+0.33}_{-0.27}$	$7.51^{+0.07}_{-0.13}$

Note. Flat uninformative or Jeffrey priors on the parameters were added to the likelihood function.

Table D5

1σ Credible Regions and the the Maximum a Posterior Estimator for the Hyperparameters Derived by the Analysis Adopting the RQ × CS Kernel for the High-energy (HE) and the Optical (Opt) Light Curves

Source	Band	$\ln A$	$\ln \alpha$	$\ln L$	$\ln P$
PG 1553 + 113	HE	$-1.93^{+1.03}_{-0.52}$	$-2.79^{+0.93}_{-1.34}$	$3.58^{+0.69}_{-0.94}$	$6.67^{+0.04}_{-0.03}$
	Opt	$1.58^{+0.79}_{-0.38}$	$-2.13^{+0.63}_{-1.05}$	$3.85^{+0.37}_{-0.21}$	$6.71^{+0.06}_{-0.04}$
PKS 2155–304	HE	$-0.58^{+0.71}_{-0.31}$	$-2.05^{+0.75}_{-1.20}$	$2.90^{+0.39}_{-0.70}$	$6.44^{+0.13}_{-0.06}$
	Opt	$5.28^{+1.15}_{-0.64}$	$-3.02^{+0.84}_{-1.27}$	$4.20^{+0.57}_{-0.32}$	$7.55^{+0.04}_{-0.07}$

Note. Flat uninformative or Jeffrey priors on the parameters were added to the likelihood function.

Table D6

1σ Credible Regions and the the Maximum a Posterior Estimator for the Hyperparameters Derived by the Analysis Adopting the AE+CS Kernel for the High-energy (HE) and the Optical (Opt) Light Curves

Source	Band	$\ln A_{AE}$	$\ln L$	$\ln A_{CS}$	$\ln P$
PG 1553 + 113	HE	$-2.76^{+0.52}_{-0.32}$	$4.81^{+0.64}_{-0.48}$	$-3.20^{+1.31}_{-2.11}$	$6.68^{+0.03}_{-0.03}$
	Opt	$1.17^{+0.40}_{-0.32}$	$5.05^{+0.42}_{-0.34}$	$-0.66^{+1.91}_{-12.0}$	$6.69^{+0.05}_{-0.86}$
PKS 2155–304	HE	$-0.97^{+0.25}_{-0.20}$	$4.02^{+0.34}_{-0.29}$	$-11.6^{+5.9}_{-5.7}$	$6.41^{+0.03}_{-0.04}$
	Opt	$4.70^{+0.47}_{-0.31}$	$5.84^{+0.49}_{-0.33}$	$-8.84^{+7.46}_{-7.54}$	$6.09^{+1.04}_{-0.98}$

Note. Flat uninformative or Jeffrey priors on the parameters were added to the likelihood function.

Table D7

1σ Credible Regions and the Maximum a Posterior Estimator for the Hyperparameters Derived by the Analysis Adopting the RQ+CS Kernel for the High-energy (HE) and the Optical (Opt) Light Curves

Source	Band	$\ln A_{RQ}$	$\ln \alpha$	$\ln L$	$\ln A_{CS}$	$\ln P$
PG 1553 + 113	HE	$-2.37^{+1.83}_{-0.62}$	$-2.36^{+1.59}_{-2.41}$	$3.36^{+0.75}_{-1.15}$	$-2.89^{+1.39}_{-1.08}$	$6.68^{+0.02}_{-0.02}$
	Opt	$1.27^{+1.26}_{-0.42}$	$-1.48^{+0.81}_{-1.70}$	$3.69^{+0.59}_{-0.21}$	$0.26^{+1.44}_{-1.95}$	$6.70^{+0.02}_{-0.03}$
PKS 2155–304	HE	$-0.73^{+0.87}_{-0.33}$	$-0.98^{+1.05}_{-1.70}$	$3.19^{+0.30}_{-0.29}$	$-4.52^{+3.00}_{-10.5}$	$6.40^{+0.35}_{-0.84}$
	Opt	$6.11^{+2.08}_{-1.14}$	$-4.04^{+1.29}_{-2.13}$	$4.58^{+1.03}_{-0.56}$	$-8.93^{+7.58}_{-7.53}$	$6.15^{+1.03}_{-1.01}$

Note. Flat uninformative or Jeffrey priors on the parameters were added to the likelihood function.

ORCID iDs

Stefano Covino https://orcid.org/0000-0001-9078-5507
Marco Landoni https://orcid.org/0000-0003-2204-8112
Angela Sandrinelli https://orcid.org/0000-0001-5171-6197
Aldo Treves https://orcid.org/0000-0002-0653-6207

References

Ackermann, M., Ajello, M., Albert, A., et al. 2015, ApJL, 813, L41
Ait Benkhali, F., Hofmann, W., Rieger, F. M., & Chakraborty, N. 2020, A&A, 634, 120
Ambikasaran, S., Foreman-Mackey, D., Greengard, L., Hogg, D. W., & O'Neil, M. 2015, ITPAM, 38, 252
Andreon, S., & Weaver, B. 2015, Bayesian Methods for the Physical Sciences. Learning from Examples in Astronomy and Physics, Vol. 4 (Berlin: Springer)
Angus, R., Morton, T., Aigrain, S., Foreman-Mackey, D., & Rajpaul, V. 2018, MNRAS, 474, 2094
Astropy Collaboration, Price-Whelan, A. M., Sipőcz, B. M., et al. 2018, AJ, 156, 123
Astropy Collaboration, Robitaille, T. P., Tollerud, E. J., et al. 2013, A&A, 558, A33
Baluev, R. V. 2008, MNRAS, 385, 1279
Baluev, R. V. 2013, MNRAS, 436, 807
Barret, D., & Vaughan, S. 2012, ApJ, 746, 131
Bhatta, G. 2019, MNRAS, 487, 3990
Bhatta, G., & Dhital, N. 2020, ApJ, 891, 120
Bretthorst, G. L. 2003, in Frequency Estimation and Generalized Lomb–Scargle Periodograms, ed. E. D. Feigelson & G. J. Babu (New York: Springer), 309
Brewer, B. J., & Stello, D. 2009, MNRAS, 395, 2226
Byrd, R., Lu, P., Nocedal, J., & Zhu, C. 1995, SIAM Journal of Scientific Computing, 16, 1190
Camenzind, M., & Krockenberger, M. 1992, A&A, 255, 59
Caproni, A., Abraham, Z., Motter, J. C., & Monteiro, H. 2017, ApJL, 851, L39
Cavaliere, A., Tavani, M., Munar-Adrover, P., & Argan, A. 2019, ApJL, 875, L22
Cavaliere, A., Tavani, M., & Vittorini, V. 2017, ApJ, 836, 220
Chevalier, J., Sanchez, D. A., Serpico, P. D., Lenain, J.-P., & Maurin, G. 2019, MNRAS, 484, 749
Chua, A. J. K., Korsakova, N., Moore, C. J., Gair, J. R., & Babak, S. 2020, PhRvD, 101, 044027
Covino, S., Sandrinelli, A., & Treves, A. 2017, in IAU Symp. 324, New Frontiers in Black Hole Astrophysics, ed. A. Gomboc (Cambridge: Cambridge Univ. Press), 180
Covino, S., Sandrinelli, A., & Treves, A. 2019, MNRAS, 482, 1270
Cumming, A. 2004, MNRAS, 354, 1165
Cutini, S., Ciprini, S., Stamerra, A., Thompson, D. J., & Perri, M. 2016, Active Galactic Nuclei 12: A Multi-Messenger Perspective (AGN12), 58, Zenodo, doi:10.5281/zenodo.163819
Doğan, S., Nixon, C., King, A., & Price, D. J. 2015, MNRAS, 449, 1251
Durrande, N., Hensman, J., Rattray, M., & Lawrence, N., D. 2016, PeerJ Computer Science, 2, e50
Duvenaud, D., Lloyd, J. R., Grosse, R., Tenenbaum, J. B., & Ghahramani, Z. 2013, arXiv:1302.4922
Elorrieta, F., Eyheramendy, S., & Palma, W. 2019, A&A, 627, A120
Falomo, R., Giraud, E., Maraschi, L., et al. 1991, ApJL, 380, L67
Feigelson, E. D., Babu, G. J., & Caceres, G. A. 2018, FrP, 6, 80
Foreman-Mackey, D. 2016, JOSS, 1, 24
Foreman-Mackey, D., Agol, E., Ambikasaran, S., & Angus, R. 2017, AJ, 154, 220
Foreman-Mackey, D., Hogg, D. W., Lang, D., & Goodman, J. 2013, PASP, 125, 306

Frescura, F. A. M., Engelbrecht, C. A., & Frank, B. S. 2008, MNRAS, 388, 1693
Gao, F., & Han, L. 2012, Comp. Opt. and Appl., 51, 259
Gelman, A., Hill, J., & Masanao, Y. 2012, Journal of Research on Educational Effectiveness, 5, 189
Gelman, A., & Tuerlinckx, F. 2000, Computational Statistics, 15, 373
Goggans, P. M., & Chi, Y. 2004, in AIP Conf. Ser. 707, Bayesian Inference and Maximum Entropy Methods in Science and Engineering, ed. G. J. Erickson & Y. Zhai (Melville, NY: AIP), 59
Graham, M. J., Djorgovski, S. G., Stern, D., et al. 2015, MNRAS, 453, 1562
Guidorzi, C., Dichiara, S., & Amati, L. 2016, A&A, 589, A98
Hamilton, J. 1994, Time Series Analysis (Princeton, NJ: Princeton Univ. Press)
Hara, N. C., Boué, G., Laskar, J., & Correia, A. C. M. 2017, MNRAS, 464, 1220
Haywood, R. D., Collier Cameron, A., Queloz, D., et al. 2014, MNRAS, 443, 2517
Hogg, D. W., & Foreman-Mackey, D. 2018, ApJS, 236, 11
Holgado, A. M., Sesana, A., Sandrinelli, A., et al. 2018, MNRAS, 481, L74
Horne, J. H., & Baliunas, S. L. 1986, ApJ, 302, 757
Huijse, P., Estévez, P. A., Förster, F., et al. 2018, ApJS, 236, 12
Hunter, J. D. 2007, CSE, 9, 90
Israel, G. L., & Stella, L. 1996, ApJ, 468, 369
Ivezić, Ž, Connelly, A. J., VanderPlas, J. T., & Gray, A. 2014, Statistics, Data Mining, and Machine Learning in Astronomy (Princeton, NJ: Princeton Univ. Press)
Jesus, J. F., Valentim, R., Escobal, A. A., & Pereira, S. H. 2020, JCAP, 4, 53
Jones, E., Oliphant, T., Peterson, P., et al. 2001, SciPy: Open Source Scientific Tools for Python, v1.10, http://www.scipy.org/
Karamanavis, V. 2017, Galax, 5, 19
Kass, R. E., & Raftery, A. E. 1995, Journal of the American Statistical Association, 90, 773
Kelly, B. C., Bechtold, J., & Siemiginowska, A. 2009, ApJ, 698, 895
Kelly, B. C., Becker, A. C., Sobolewska, M., Siemiginowska, A., & Uttley, P. 2014, ApJ, 788, 33
Koen, C. 1990, ApJ, 348, 700
Koen, C. 2005, MNRAS, 361, 887
Kovačević, A. B., Popović, L. Č., Simić, S., & Ilić, D. 2019, ApJ, 871, 32
Kwiatkowski, D., Phillips, P., Schmidt, P., & Shin, Y. 1992, Journal of Econometrics, 54, 159
Landoni, M., Falomo, R., Treves, A., & Sbarufatti, B. 2014, A&A, 570, A126
Lehto, H. J., & Valtonen, M. J. 1996, ApJ, 460, 207
Lenoir, G., & Crucifix, M. 2018, NPGeo, 25, 145
Li, Y.-R., & Wang, J.-M. 2018, MNRAS, 476, L55
Lico, R., Liu, J., Giroletti, M., et al. 2020, A&A, 634, A87
Liddle, A. R. 2007, MNRAS, 377, L74
Lindfors, E. J., Hovatta, T., Nilsson, K., et al. 2016, A&A, 593, A98
Littlefair, S. P., Burningham, B., & Helling, C. 2017, MNRAS, 466, 4250
Lomb, N. R. 1976, Ap&SS, 39, 447
Luger, R., Agol, E., Kruse, E., et al. 2016, AJ, 152, 100
Marscher, A. P. 2014, ApJ, 780, 87
Milotti, E. 2002, arXiv:physics/0204033
Milotti, E. 2007, PhRvE, 75, 011120
Nilsson, K., Lindfors, E., Takalo, L. O., et al. 2018, A&A, 620, A185
Oliphant, T. 2006, NumPy: A guide to NumPy (USA: Trelgol Publishing), http://www.numpy.org/
Pereira, F., Campante, T. L., Cunha, M. S., et al. 2019, MNRAS, 489, 5764
Press, W. H. 1978, ComAp, 7, 103
Prokhorov, D. A., & Moraghan, A. 2017, MNRAS, 471, 3036
Raiteri, C. M., Villata, M., Acosta-Pulido, J. A., et al. 2017, Natur, 552, 374
Rajpaul, V., Aigrain, S., Osborne, M. A., Reece, S., & Roberts, S. 2015, MNRAS, 452, 2269
Rasmussen, C. E., & Williams, C. K. I. 2006, Gaussian Processes for Machine Learning (Cambridge, MA: MIT Press)
Rieger, F. 2019, Galax, 7, 28
Roberts, S., Osborne, M., Ebden, M., et al. 2012, RSPTA, 371, 20110550
Ryan, J. L., Siemiginowska, A., Sobolewska, M. A., & Grindlay, J. 2019, ApJ, 885, 12
Sandrinelli, A., Covino, S., Dotti, M., & Treves, A. 2016a, AJ, 151, 54
Sandrinelli, A., Covino, S., & Treves, A. 2014, ApJL, 793, L1
Sandrinelli, A., Covino, S., & Treves, A. 2016b, ApJ, 820, 20
Sandrinelli, A., Covino, S., Treves, A., et al. 2017, A&A, 600, A132
Sandrinelli, A., Covino, S., Treves, A., et al. 2018, A&A, 615, A118
Scargle, J. D. 1982, ApJ, 263, 835
Schwarz, G. 1978, AnSta, 6, 461
Schwarzenberg-Czerny, A. 1997, ApJ, 489, 941
Schwarzenberg-Czerny, A. 1998, MNRAS, 301, 831
Sharma, S. 2017, ARA&A, 55, 213
Sobacchi, E., Sormani, M. C., & Stamerra, A. 2017, MNRAS, 465, 161
Stamerra, A., Prandini, E., Paiano, S., et al. 2016, Active Galactic Nuclei 12: A Multi-Messenger Perspective (AGN12), 64, Zenodo, doi:10.5281/zenodo.163826
Stellingwerf, R. F. 1978, ApJ, 224, 953
Sulis, S., Mary, D., & Bigot, L. 2017, ITSP, 65, 2136
Süveges, M. 2014, MNRAS, 440, 2099
Süveges, M., Guy, L. P., Eyer, L., et al. 2015, MNRAS, 450, 2052
Tak, H., Ghosh, S. K., & Ellis, J. A. 2018, MNRAS, 481, 277
Takata, T., Mukuta, Y., & Mizumoto, Y. 2018, ApJ, 869, 178
Tavani, M., Cavaliere, A., Munar-Adrover, P., & Argan, A. 2018, ApJ, 854, 11
Tobar, F. 2018, in NIPS 2018, Advances in Neural Information Processing Systems 31, ed. S. Bengio et al. (Red Hook, NY: Curran Associates, Inc.) https://papers.nips.cc/paper/8216-bayesian-nonparametric-spectral-estimation
Tobar, F., Bui, T. D., & Turner, R. E. 2015, in NIPS 2015, Advances in Neural Information Processing Systems 28, ed. C. Cortes et al. (Red Hook, NY: Curran Associates, Inc.), https://papers.nips.cc/paper/5772-learning-stationary-time-series-using-gaussian-processes-with-nonparametric-kernels
Trotta, R. 2007, MNRAS, 378, 72
Trotta, R. 2008, ConPh, 49, 71
Urry, M. 2012, AstRv, 7, 4
Uttley, P., McHardy, I. M., & Papadakis, I. E. 2002, MNRAS, 332, 231
van der Klis, M. 1989, ARA&A, 27, 517
van Rossum, G. 1995, Python tutorial, Tech. Rep. CS-R9526, Centrum voor Wiskunde en Informatica (CWI), Amsterdam
Vanderburg, A., Montet, B. T., Johnson, J. A., et al. 2015, ApJ, 800, 59
VanderPlas, J. T. 2018, ApJS, 236, 16
Vaughan, S. 2010, MNRAS, 402, 307
Vaughan, S. 2012, RSPTA, 971, 20110549
Vaughan, S., Uttley, P., Markowitz, A. G., et al. 2016, MNRAS, 461, 3145
Vio, R., & Andreani, P. 2018, arXiv:1807.01595
Wang, Y., Khardon, R., & Protopapas, P. 2012, ApJ, 756, 67
Wilkins, D. R. 2019, MNRAS, 489, 1957
Wilson, A. G., & Prescott Adams, R. 2013, arXiv:1302.4245
Zechmeister, M., & Kürster, M. 2009, A&A, 496, 577
Zhang, B.-K., Zhao, X.-Y., Wang, C.-X., & Dai, B.-Z. 2014, RAA, 14, 933
Zhang, P.-f., Yan, D.-h., Liao, N.-h., et al. 2017a, ApJ, 842, 10
Zhang, P.-f., Yan, D.-h., Liao, N.-h., & Wang, J.-c. 2017b, ApJ, 835, 260
Zhang, P.-F., Yan, D.-H., Zhou, J.-N., et al. 2017c, ApJ, 845, 82